Title
CRACR2a is a calcium-activated dynein adaptor protein that regulates endocytic traffic

Journal
Journal of Cell Biology, 218(5)

ISSN
0021-9525

Authors
Wang, Yuxiao
Huynh, Walter
Skokan, Taylor D
et al.

Publication Date
2019-05-06

DOI
10.1083/jcb.201806097

Peer reviewed

JCB Journal of Cell Biology

ARTICLE

CRACR2a is a calcium-activated dynein adaptor protein that regulates endocytic traffic

Yuxiao Wang[1,2], Walter Huynh[1,2], Taylor D. Skokan[1,2], Wen Lu[3], Arthur Weiss[2,3], and Ronald D. Vale[1,2]

Cytoplasmic dynein is a minus end–directed microtubule motor that transports intracellular cargoes. Transport is initiated by coiled-coil adaptors that (a) join dynein and its cofactor dynactin into a motile complex and (b) interact with a cargo-bound receptor, which is frequently a Rab GTPase on an organelle. Here, we report two novel dynein adaptors, CRACR2a and Rab45, that have a coiled-coil adaptor domain, a pair of EF-hands, and a Rab GTPase fused into a single polypeptide. CRACR2a-mediated, but not Rab45-mediated, dynein motility is activated by calcium in vitro. In Jurkat T cells, elevation of intracellular calcium activates CRACR2a-mediated dynein transport. We further found that T cell receptor activation induces the formation of CRACR2a puncta at the plasma membrane, which initially associate with the actin cortex and subsequently detach and travel along microtubules, suggestive of an endocytic process. These results provide the first examples of Rab GTPases that directly act as dynein adaptors and implicate CRACR2a–dynein in calcium-regulated endocytic trafficking.

Introduction

Microtubule-based transport is essential for the positioning of large membrane organelles, the trafficking of small transport vesicles, and the localization of mRNA and protein (Schliwa and Woehlke, 2003; Vale, 2003). Microtubules are polarized filaments with distinct plus and minus ends; in most cells, microtubule plus ends extend to the cell periphery and minus ends are anchored to the microtubule-organizating center (MTOC). Plus end–directed transport is mediated by kinesin, a large family of motor proteins with >40 members in mammals (Hirokawa et al., 2009). In contrast, all minus end–directed intracellular transport in animal cells is performed by a single motor protein complex, cytoplasmic dynein-1 (referred to as dynein hereafter; Vale, 2003; Reck-Peterson et al., 2018). Most, if not all, membrane organelles are transported by dynein (Reck-Peterson et al., 2018).

The dynein holoenzyme is composed of an ∼500-kD heavy chain and five smaller subunits (three light chains, one light-intermediate chain, and one intermediate chain). Mammalian dynein does not display processive motility, owing to autoinhibition of its motor domain (Zhang et al., 2017). Binding of the dynactin complex and an adaptor protein activates dynein, enabling it to move processively along microtubules (McKenney et al., 2014; Schlager et al., 2014). Thus far, eight adaptors have been demonstrated to directly bind and activate dynein: BicDL1, BicD2, Hook1, Hook3, Rab11FIP3, Spindly, Ninein, and Ninein-like protein (Reck-Peterson et al., 2018). A common feature of these proteins is the presence of long coiled-coil domains. Structural studies revealed that the coiled-coils of BicD and Hook are directly involved in joining dynein and dynactin together into a tripartite complex (Urnavicius et al., 2015, 2018).

Recruitment of the dynein–dynactin adaptor complex to specific membrane organelles is often mediated by the interaction between a dynein adaptor and a Rab GTPase, which associates with intracellular membrane compartments through C-terminal prenylation (Hutagalung and Novick, 2011; Reck-Peterson et al., 2018). Rab GTPases have been shown to regulate the localization as well as the conformation of dynein adaptors. Rab6, which localizes to Golgi-derived vesicles, recruits the dynein adaptor BicD to mediate retrograde transport (Matanis et al., 2002). Binding of Rab6 to BicD also alleviates its autoinhibition and promotes BicD-mediated dynein–dynactin activation (Hoogenraad et al., 2003; Liu et al., 2013; Huynh and Vale, 2017). Thus far, no Rab has been shown to possess the ability to interact with and activate dynein–dynactin directly.

Here, we report the discovery of two novel dynein adaptor proteins, Rab45 and CRACR2a, both of which are also Rab GTPases (Srikanth et al., 2017). These are the first identified dynein–dynactin adaptors that contain both a Rab GTPase

[1]Department of Cellular and Molecular Pharmacology, University of California, San Francisco, San Francisco, CA; [2]Howard Hughes Medical Institute, University of California, San Francisco, San Francisco, CA; [3]Division of Rheumatology, Rosalind Russell and Ephraim P. Engleman Arthritis Research Center, Department of Medicine, University of California, San Francisco, San Francisco, CA.

Correspondence to Ronald D. Vale: ron.vale@ucsf.edu.

domain and a coiled-coiled dynein–dynactin activator domain. We found that the ability of CRACR2a to activate dynein–dynactin is stimulated by physiological concentrations of calcium. CRACR2a was initially identified as a 46-kD cytosolic protein that regulates CRAC channel activation in T cells (Srikanth et al., 2010). Subsequently, a longer 90-kD isoform of CRACR2a was identified that localizes to vesicles that translocate toward the immunological synapse (IS) and regulate JNK activation downstream of the T cell receptor (TCR; Srikanth et al., 2016). Examining the localization of the long isoform of CRACR2a in activated Jurkat T cells, we found an additional population of CRACR2a that forms distinct puncta that migrate with actin retrograde flow at the IS and that require microtubules to detach from the actin cortex and move toward the MTOC. We provide evidence suggesting that the formation of CRACR2a puncta is a clathrin-independent process, and that CRACR2a may be involved in the endocytic transport of the cell surface molecule CD47. Together, our results demonstrate that Rab45 and CRACR2a constitute a new class of dynein adaptors and reveal a role of CRACR2a and dynein in endocytic traffic.

Results

Identification of Rab45 and CRACR2a as activating adaptors for dynein

Rab45 and CRACR2a are atypical Rab GTPases that contain a pair of EF-hand domains, a coiled-coil domain, and a Rab GTPase domain (Fig. 1 A). We speculated that these proteins may function as dynein adaptor proteins due to (a) their domain architecture (EF-hands followed by coiled-coils), which resembles that of known dynein adaptors, such as Rab11FIP3 and Ninein (Fig. 1 A), and (b) their localization to a small, perinuclear compartment at the cell center, suggestive of microtubule minus end–directed transport (Shintani et al., 2007; Srikanth et al., 2016). The human CRACR2a gene was shown to undergo alternative splicing to produce two isoforms (Wilson et al., 2015; Srikanth et al., 2016). In this study, we focused on the long isoform, as the short isoform lacks the Rab GTPase domain and does not seem to be involved in membrane trafficking (Srikanth et al., 2016).

We first sought to determine whether Rab45 and CRACR2a could interact with dynein and dynactin. To this end, we expressed and purified Rab45 and CRACR2a fused with a Strep-tag and superfolder GFP (Fig. S1 A), attached these proteins to StrepTactin beads, and then performed pulldown assays with dynein–dynactin isolated from RPE1 cells. Indeed, both Rab45 and CRACR2a interacted with dynein–dynactin in these pulldown assays (Fig. 1 B).

We next examined the ability of Rab45 and CRACR2a to activate the processive motility of native dynein–dynactin using an established total internal reflection fluorescence (TIRF) microscopy single-molecule assay (McKenney et al., 2014; Huynh and Vale, 2017). Purified Rab45 and CRACR2a robustly activated the processive motility of dynein–dynactin on microtubules (Fig. 1, C and D), similar to other known dynein adaptors (McKenney et al., 2014; Schlager et al., 2014; Redwine et al., 2017). The velocities of movement were 0.99 ± 0.21 µm/s and 0.67 ± 0.25 µm/s (mean ± SD) for Rab45 and CRACR2a, respectively. Together, these data indicate that Rab45 and CRACR2a can bind to dynein–dynactin and activate dynein motility in vitro.

To determine whether Rab45 and CRACR2a activate dynein transport in cells, we employed a previously developed inducible peroxisome trafficking assay, in which a candidate adaptor protein is induced to localize to peroxisomes by addition of rapamycin (Kapitein et al., 2010; Fig. 1 E). In the absence of rapamycin, peroxisomes are distributed randomly throughout the cell (Fig. 1 F). Recruitment of a dynein adaptor to peroxisomes causes them to move toward the microtubule minus end and accumulate around the MTOC (Fig. 1 E). We found that rapamycin-induced targeting of Rab45 and CRACR2a to peroxisomes resulted in strong clustering of peroxisomes at the cell center (Fig. 1 F), suggesting that Rab45 and CRACR2a are capable of recruiting dynein and activating dynein-mediated transport in cells.

Regulation of the dynein adaptor function of Rab45 and CRACR2a by calcium

The presence of EF-hands, a known calcium binding motif, in Rab45 and CRACR2a led us to examine whether calcium regulates their function as dynein adaptors. In the previous pulldown and single-molecule assays (Fig. 1, B and C), we did not add calcium or EGTA, in which case trace amounts of calcium at micromolar levels could still be present in the buffer (Bers et al., 2010). We therefore repeated the dynein–dynactin binding assay either with 2 mM EGTA, to deplete calcium completely, or with 2 µM free calcium (buffered by EGTA:Ca^{2+}), a concentration relevant for most calcium-dependent physiological processes (Bers et al., 2010; see Materials and methods for details). While complex formation between Rab45 and dynein–dynactin was insensitive to calcium, CRACR2a required the presence of calcium for stable interaction with dynein and dynactin (Fig. 2 A). In addition, mutating the calcium binding sites in the EF-hands of CRACR2a ($CRACR2A^{EFmut}$) abolished its interaction with dynein–dynactin, regardless of calcium concentration (Fig. 2 A).

We further tested whether the single-molecule motility of CRACR2a–dynein–dynactin responds to changes of calcium in the physiological range (100 nM to ∼10 µM). Raising calcium concentration from 10 nM to 2 µM significantly increased the number of processive events on microtubules (Fig. 2 B), consistent with the calcium-dependent stabilization of CRACR2a–dynein–dynactin complex as shown in the pulldown assay. In contrast, the motility of Rab45-dynein–dynactin was similar in the presence of EGTA or 2 µM calcium (Fig. S1). Taken together, these results suggest that the dynein adaptor function of CRACR2a is activated by physiological levels of calcium.

T cell activation–induced calcium elevation stimulates the transport of CRACR2a toward the MTOC

Intrigued by the regulation of CRACR2a-mediated dynein motility by calcium in vitro, we decided to further pursue in vivo studies of this adaptor protein. CRACR2a is highly expressed in primary T cells as well as in the Jurkat T cell line (Srikanth et al., 2016). We observed that GFP-CRACR2a stably expressed in

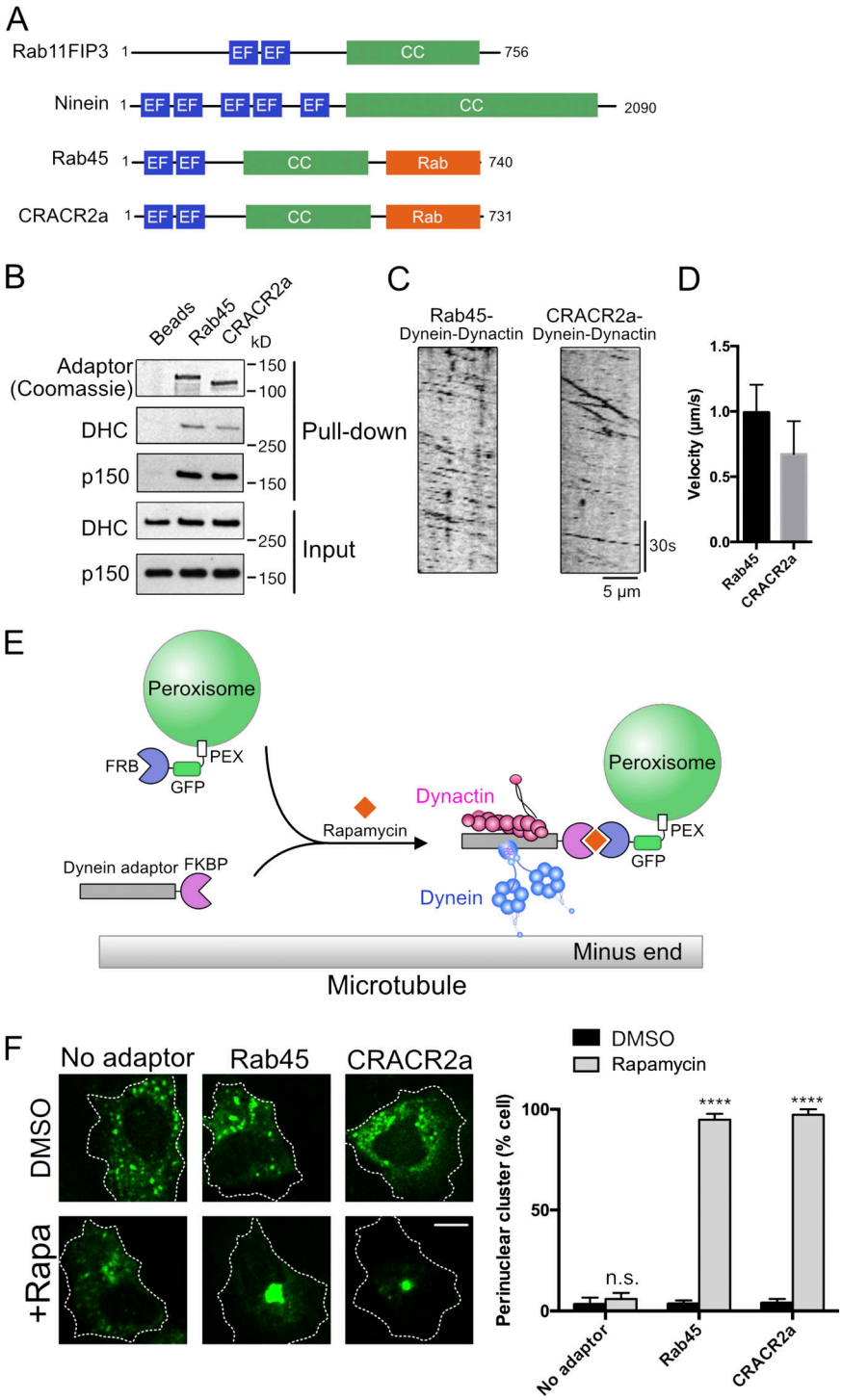

Figure 1. **Rab45 and CRACR2a are adaptor proteins for dynein. (A)** Domain organizations of Rab45, CRACR2a, Rab11FIP3, and Ninein. EF, EF-hand; CC, coiled-coil. Sizes of the domains are not to scale. **(B)** Pulldown assay shows that Rab45 and CRACR2a bind to dynein–dynactin. DHC, dynein heavy chain; p150, the p150 subunit of dynactin. Western bands are from the same gel. **(C)** Sample kymographs of microtubule-based motility of Rab45 or CRACR2a in complex with dynein–dynactin. Fluorescence is from the N-terminal GFP tag on Rab45 or CRACR2a. **(D)** Quantification of the velocities of dynein–dynactin in complex with Rab45 or CRACR2a. Error bar: SD; n = 40 processive particles from three replicates. **(E)** Schematic of the inducible peroxisome trafficking assay. U2OS cells were transfected to express GFP-FRB fused with a peroxisome targeting sequence (PEX) and an mCherry-adaptor-FKBP construct. Treatment of the cell with rapamycin induces the localization of the dynein–dynactin adaptor complex to peroxisomes and drives retrograde transport of peroxisomes toward the microtubule minus end. **(F)** Representative images of the peroxisome transport assay (scale bar: 10 µm). +Rapa, treatment with rapamycin. Quantifications of the percentage of cells with a strong perinuclear cluster of peroxisomes are shown on the right. Data are mean ± SEM of three independent experiments (n = 30–40 cells per experiment). ****, $P < 0.0001$ between DMSO-treated group and rapamycin-treated group using two-way ANOVA analysis with Sidak's multiple comparisons test.

Jurkat localized to a loosely connected membrane compartment surrounding the MTOC (Fig. 3 A), as well as to small vesicles that traveled bidirectionally along microtubules, consistent with observations made by Srikanth et al. (2016) (Video 1 and Fig. 3 A). We also found GFP-CRACR2a diffusely localized throughout the cytoplasm (Video 1 and Fig. 3 A). Western blot with endogenous antibody showed that GFP-CRACR2a remained full length and was expressed at roughly the same level of the endogenous CRACR2a, suggesting that the cytosolic CRACR2a was not due to protein degradation or overexpression (Fig. S2 B). It is possible that the cytosolic CRACR2a was GDP bound and unable to associate with membrane, as shown by Srikanth et al. (2016).

We next sought to examine whether CRACR2a in Jurkat T cells responds to changes in intracellular calcium. The GFP-CRACR2a vesicular compartment was loosely associated with the MTOC in resting Jurkat cells (Fig. 3 A). Treatment of the cells with ionomycin, which elevates cytoplasmic calcium, caused GFP-CRACR2a to further concentrate at a small region adjacent to the MTOC (Fig. 3, A and B). To test if the EF-hands in CRACR2a are responsible for such calcium-dependent MTOC congregation,

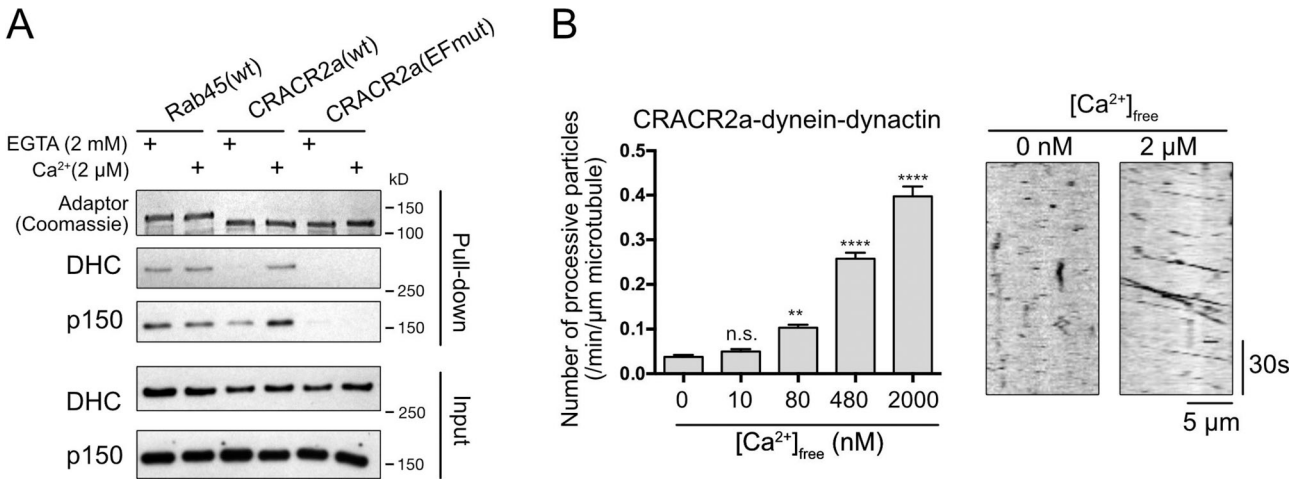

Figure 2. **Regulation of the dynein adaptor function of CRACR2a by calcium. (A)** Dynein–dynactin pulldown assays performed with calcium-depleted buffer (2 mM EGTA) or buffer containing 2 µM free calcium. DHC, dynein heavy chain; p150, the p150 subunit of dynactin. Western bands are from the same gel. **(B)** Quantification of CRACR2a–dynein–dynactin motility at different free calcium concentrations. Data were collected from three replicates, with each calcium condition measuring at least 25 microtubules. Error bar: SEM. **, P < 0.01; ****, P < 0.0001, one-way ANOVA and Dunnett's test versus zero free calcium condition. Example kymographs are shown on the right.

we generated a CRACR2a knockout Jurkat cell line, J.CRACR2a, using CRISPR/Cas9 (Fig. S2), and reintroduced GFP-CRACR2a^{EFmut}. Disruption of the calcium-binding sites in the EF-hands completely abolished ionomycin-induced MTOC clustering of GFP-CRACR2a (Fig. 3, B and C), consistent with the in vitro observation that CRACR2a^{EFmut} failed to bind to dynein–dynactin (Fig. 2 A). To test the notion that the calcium-stimulated accumulation of CRACR2a at the MTOC is caused by an increase of retrograde transport of CRACR2a-bound vesicles (and not cytosolic GFP-CRACR2a), we expressed a GFP-CRACR2a mutant lacking the C-terminal polybasic region and prenylation motif (GFP-CRACR2a$^{\Delta tail}$) in wild-type Jurkat cells. As expected, GFP-CRACR2a$^{\Delta tail}$ was completely diffusive in the cytoplasm (Fig. 3 B). Moreover, ionomycin treatment failed to induce clustering of GFP-CRACR2a$^{\Delta tail}$ at the MTOC (Fig. 3, B and C), suggesting that membrane association of CRACR2a mediated by prenylation is essential for the observed accumulation of CRACR2a at the MTOC in response to calcium elevation.

TCR activation induces a rapid increase of intracellular free calcium to initiate downstream signaling. To determine if CRACR2a dynamics are altered during TCR triggering, we stimulated Jurkat cells expressing GFP-CRACR2a with immobilized anti-CD3ε antibody (clone OKT3). T cell activation induced a rapid congregation of GFP-CRACR2a at the MTOC (Fig. 3, D and E), similar to what was observed with ionomycin treatment. Chelation of extracellular and intracellular calcium by EGTA and BAPTA, as well as mutation of the calcium-binding sites in the EF-hands of CRACR2a, abolished the ability of TCR activation to cause CRACR2a clustering at the MTOC (Fig. 3, D and E). These results indicate that, in response to calcium increase induced by TCR activation, CRACR2a recruits and activates dynein to undergo retrograde transport toward the MTOC.

Activation of a T cell by an antigen-presenting cell leads to the formation of a specialized cell–cell junction known as the IS (Dustin et al., 2010). A previous study reported that during T cell activation CRACR2a vesicles translocate toward the IS (Srikanth et al., 2016). We stimulated Jurkat cells with immobilized anti-CD3 and examined the dynamics of CRACR2a at the IS using TIRF microscopy, which only illuminates regions adjacent to the basal cell membrane. We observed that the MTOC and the vesicular compartment of CRACR2a migrated together into the TIRF field and docked at the center of the IS (Fig. S3 B). This suggests that the previously reported translocation of GFP-CRACR2a is likely due to the movement of the MTOC toward the IS, which brings with it most of the microtubule network and the endomembrane system (Stinchcombe and Griffiths, 2014).

We sought to determine whether the CRACR2a vesicular compartment at the MTOC colocalizes with known membrane organelles. An earlier study suggested that CRACR2a colocalized with the Rab8-positive trans-Golgi network in T cells (Srikanth et al., 2016). Although GFP-CRACR2a and mCherry-Rab8 in Jurkat cells both localized to the perinuclear region, high-resolution confocal imaging revealed little colocalization between the two proteins (Fig. S4 A). In addition, ionomycin treatment did not change the distribution of Rab8A, whereas it strongly compacted CRACR2a-containing membrane compartments at the MTOC (Fig. S4, A and B). We further tested the colocalization between CRACR2a and Rab11A, which localizes to perinuclear recycling endosomes. In the basal state, CRACR2a appears to partially colocalize with Rab11A (Fig. S4 C). However, upon ionomycin stimulation, only CRACR2a, and not Rab11A, relocalized and became tightly clustered at the MTOC (Fig. S4, C and D). These results together suggest that the subcellular localization of CRACR2a is distinct from that of Rab8 or Rab11.

T cell activation promotes the formation of CRACR2a puncta at the cell cortex

When examining the dynamics of CRACR2a at the IS by TIRF microscopy, we also observed the formation of dim and

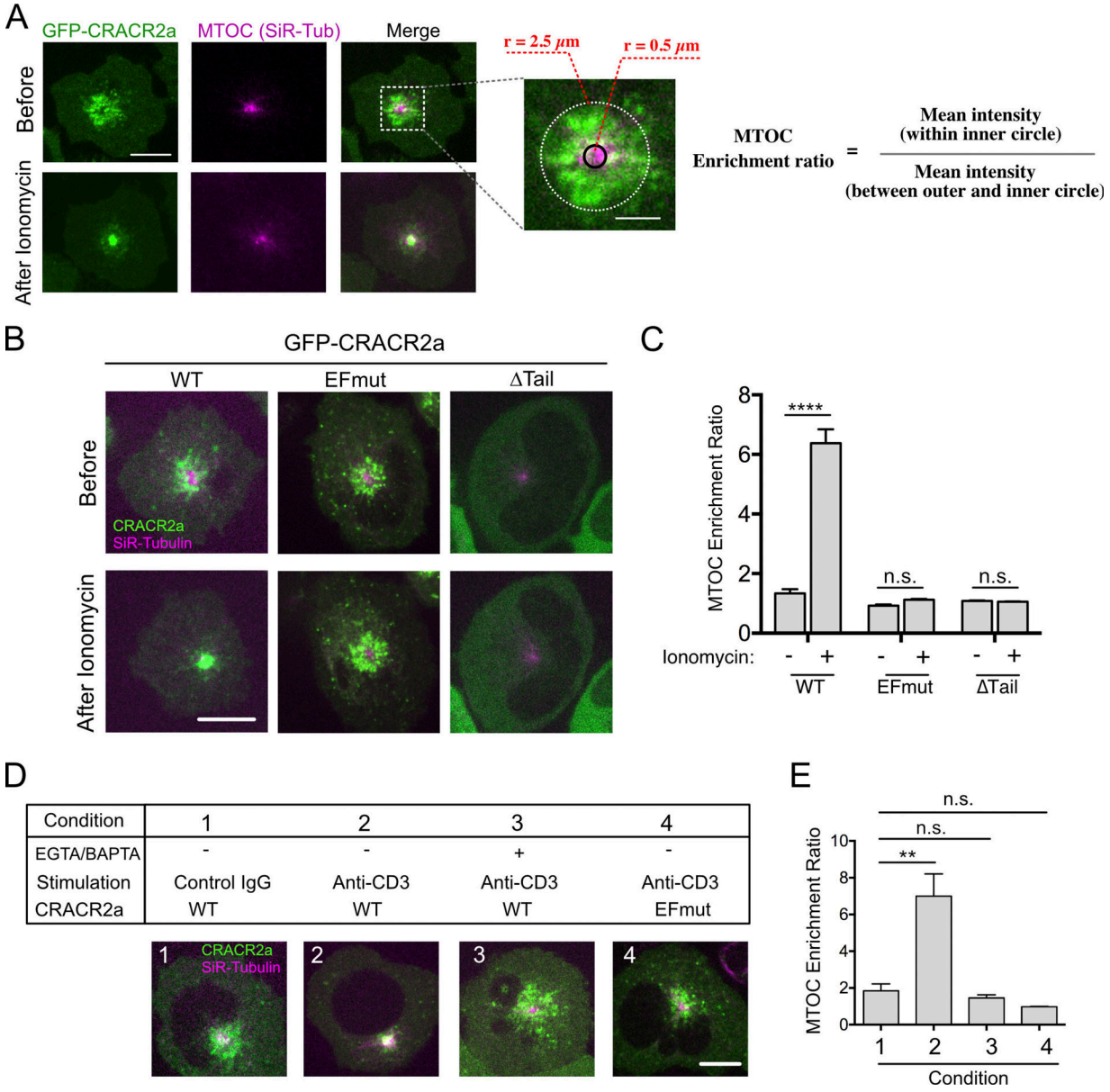

Figure 3. **Calcium regulation of CRACR2a subcellular localization in T cells. (A)** Changes in CRACR2a localization before and after ionomycin treatment, as well as the method used for quantification of the distribution of CRACR2a adjacent to the MTOC. The same cell before and after ionomycin treatment is shown. MTOC is visualized by staining with 100 nM SiR-Tubulin for 4 h and adjusting the intensity scale of the image to show only high-intensity pixels (see Fig. S3 A). MTOC enrichment ratio is defined as the ratio of mean GFP intensity within a 0.5-µm region of the MTOC versus the mean GFP intensity within a 0.5-µm to ∼2.5-µm region of the MTOC. Scale bar: 5 µm. Inset scale bar: 1 µm. **(B)** Mutational study of CRACR2a clustering at the MTOC. EFmut, J.CRACR2a cell line expressing GFP-CRACR2a with mutated calcium-binding site in EF-hands (D63A, E65A, D97A, D99A). ΔTail, wild-type Jurkat line expressing GFP-CRACR2a with a deletion of C-terminal tail (Δ725–731). Scale bar: 10 µm. **(C)** Quantifications of relative enrichment of CRACR2a at the MTOC for experiments shown in B. Data are mean ± SEM of three independent experiments (n = 11–30 cells per group in each experiment). ****, $P < 0.0001$, two-way ANOVA with Sidak's multiple comparisons test. **(D)** T cell activation induces clustering of CRACR2a compartments at the MTOC. Scale bar: 10 µm. **(E)** Quantifications of the levels of relative enrichment at MTOC for experiments shown in D. Data are mean ± SEM of three independent experiments (n = 10–30 cells per group in each experiment). **, $P < 0.01$, one-way ANOVA with Dunnett's test comparing each sample with sample #1.

diffraction-limited GFP-CRACR2a puncta at the cell periphery (Fig. 4 A). These puncta were difficult to resolve under a confocal microscope, but visible when imaged using TIRF microscopy, suggesting that they are at or adjacent to the plasma membrane. Notably, these puncta were morphologically distinct from the CRACR2a vesicular compartments described earlier, which are relatively large and enter into the TIRF field at the center of the cell (Fig. S3 B). We refer to the plasma membrane localized CRACR2a as "cortical puncta" to distinguish them from the pool of CRACR2a localized to intracellular vesicles.

To determine whether T cell signaling regulates the formation of CRACR2a cortical puncta, we plated Jurkat cells onto isotype control antibody-coated glass and observed very few cortical puncta at the cell membrane (Fig. 4 B). Addition of

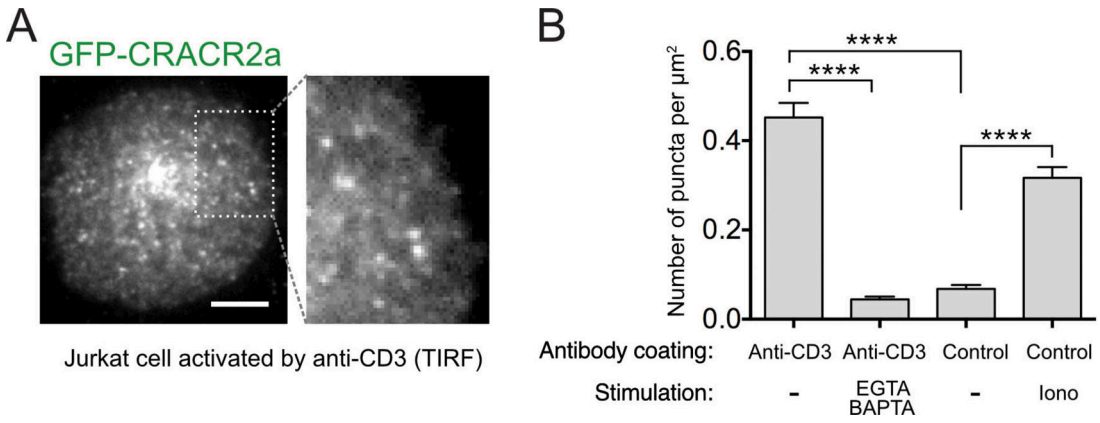

Figure 4. **T cell activation promotes the formation of CRACR2a puncta at the cell cortex. (A)** Formation of CRACR2a cortical puncta at the periphery of the IS. Scale bar: 5 µm. **(B)** Quantification of the number of observed CRACR2a cortical puncta when Jurkat cells are stimulated by different conditions. Control, IgG isotype control; Iono, stimulation with ionomycin/calcium. *n* = 29–41 ROIs from at least 20 cells collected during three independent experiments. Error bar indicates SEM. ****, P < 0.0001, one-way ANOVA with Tukey's multiple comparisons test.

ionomycin in this condition stimulated the formation of the cortical puncta (Fig. 4 B). In contrast, depletion of both extracellular and cytoplasmic calcium by EGTA/BAPTA blocked the formation of cortical puncta when cells were activated by immobilized anti-CD3 (Fig. 4 B). These results suggest that the formation of CRACR2a cortical puncta at the IS is stimulated by TCR activation–induced calcium elevation.

CRACR2a cortical puncta are distinct from previously characterized endosomal and Golgi-derived vesicles

To further explore the identity of the CRACR2a cortical puncta, we examined whether they colocalize with markers for different endosomal populations, including clathrin light-chain (clathrin-coated pits and vesicles), Rab5A (early endosomes), Rab11A (recycling endosomes), and Rab22A and Arf6 (clathrin-independent endosomes; Ferreira and Boucrot, 2017; Johnson et al., 2017). We did not observe colocalization between the cortical puncta and any of these markers (Fig. 5 A). Srikanth et al. (2016) also reported that CRACR2a forms vesicles that translocate from the Golgi to the IS. To test whether the cortical puncta are Golgi-derived transport vesicles, we blocked post-Golgi trafficking with Brefeldin A (Miller et al., 1992). The formation of CRACR2a cortical puncta was not affected by Brefeldin A treatment, suggesting that they are not Golgi-derived vesicles (Fig. 5 B).

We further treated the cells with a panel of chemical inhibitors that disrupt clathrin-coated pit formation (chlorpromazine or PitSTOP2) or caveolae-mediated uptake (Filipin III). None of these inhibitors affected the number of the cortical puncta observed (Fig. 5 B). In contrast, inhibition of actin polymerization (with 2 µM latrunculin A [LatA] or 5 µM cytochalasin B) completely abolished the appearance of CRACR2a cortical puncta (Fig. 5 B). Dynamin GTPases are involved in the formation of clathrin-dependent and a subset of clathrin-independent endosomes (Doherty and McMahon, 2009). Inhibition of dynamin function by overexpression of the K44A dominant-negative mutant of dynamin (DynK44A) caused a 40% reduction of the number of the cortical puncta, while MiTMAB, a chemical inhibitor of dynamin function, did not have any effect, indicating that the formation of the cortical puncta could be partially dynamin dependent (Fig. 5 B). Together, these results suggest that the CRACR2a cortical puncta are formed through a clathrin-independent, caveolin-independent but actin-dependent pathway.

CRACR2a cortical puncta comigrate with F-actin retrograde flow at the IS

The CRACR2a cortical puncta in the TIRF field emerged from the distal edge of the lamella and migrated centripetally (Fig. 6 A and Video 2). Activation of the TCR leads to rapid polymerization of F-actin at the perimeter of the IS, resulting in robust retrograde actin flow (Yi et al., 2012). To understand the relation of CRACR2a cortical puncta to actin, we visualized both GFP-CRACR2a and mCherry-F-tractin, a probe for filamentous actin (Yi et al., 2012). The cortical puncta comigrated with the retrograde flow of actin at the IS (Fig. 6 A and Video 3) with similar speeds (cortical puncta, 0.068 ± 0.023 µm/s; F-actin, 0.065 ± 0.025 µm/s, mean ± SD; Fig. 6 B). Disruption of F-actin using LatA (2 µM) rapidly abolished the formation of new cortical puncta, as well as the centripetal movement of preexisting cortical puncta (Fig. 6 A and Video 4). These results suggest that actin is involved in the formation of CRACR2a cortical puncta and drives their retrograde flow to the center of the IS.

CRACR2a cortical puncta recruit dynein to detach from the actin cortex and travel to the MTOC

Given our earlier result that CRACR2a is an adaptor for dynein, we wondered whether dynein was recruited to CRACR2a cortical puncta. Coexpression of mCherry-tagged dynein light chain Tctex3 showed that dynein localized to the cortical puncta immediately after their appearance at the edge of the cell (Fig. 7 A and Video 5). We reexamined the dynamics of the cortical puncta using a spinning disk confocal microscope with fluorescent labeling of actin and microtubules. High cytosolic fluorescence signal and fast photobleaching precluded precise tracking of the movement of each punctum. Nevertheless,

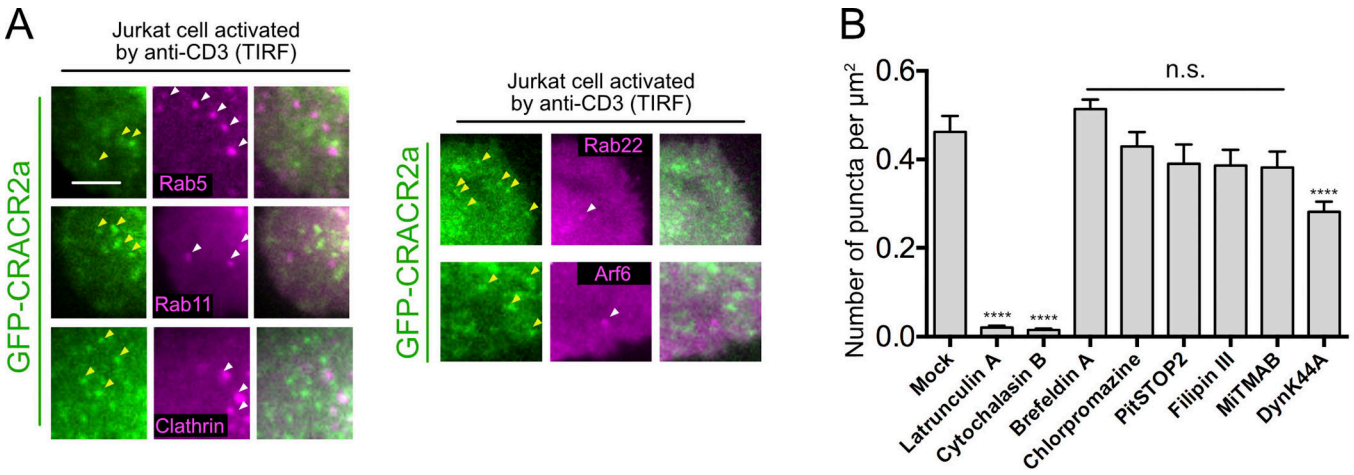

Figure 5. **CRACR2a cortical puncta are distinct from previously characterized endosomal and Golgi-derived vesicles. (A)** CRACR2a cortical puncta (indicated by yellow arrowheads) do not colocalize with Rab5, Rab11, Rab22, Arf6, or clathrin-coated pits (indicated by white arrowheads). Scale bar: 3 µm. **(B)** Quantifications of the number of CRACR2a puncta observed in activated Jurkat cells under different treatments. DynK44A, coexpression of the K44A dominant-negative mutant of dynamin 1; *n* = 15–48 ROIs from at least 20 cells collected during three independent experiments. Error bar indicates SEM. ****, P < 0.0001, one-way ANOVA with Dunnett's multiple comparisons test comparing each sample with mock (DMSO) treated sample.

occasionally we could observe that a slowly migrating CRACR2a cortical punctum abruptly switched to fast retrograde movement on microtubules toward the MTOC (Fig. 7 B). Depolymerization of microtubules by nocodazole treatment did not affect the retrograde movement of CRACR2a cortical puncta at the peripheral region of the IS (Video 6). However, under these conditions, CRACR2a failed to form a tight cluster at the MTOC, but instead accumulated within the TIRF field (<200-nm zone near the plasma membrane) at the actin-depleted region of the IS to form a disk-like structure (Fig. 7 C and Video 6). Further disruption of F-actin in nocodazole-treated cells caused the accumulated cortical puncta to disperse from the disk-like structure (Fig. 7 C), suggesting that the cortical puncta remain associated with the actin cortex when microtubules are absent. Taken together, the above results indicate that microtubule-based transport is important for the cortical puncta to dissociate from the actin cortex and move toward the MTOC.

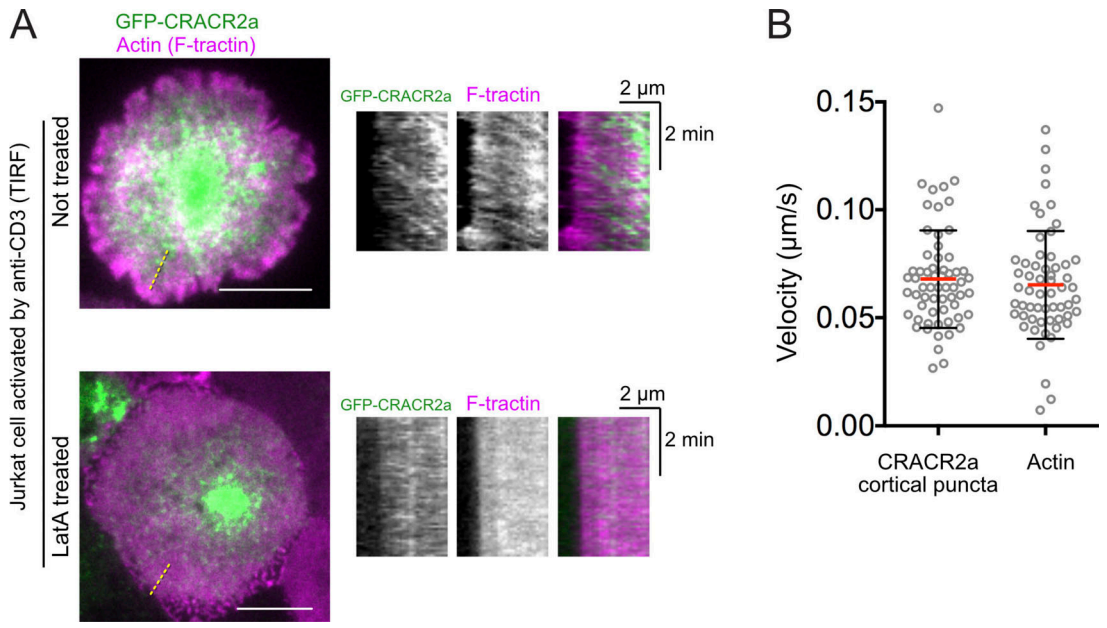

Figure 6. **CRACR2a cortical puncta comigrate with F-actin retrograde flow at the IS. (A)** GFP-CRACR2a puncta migrate with actin retrograde flow. GFP-CRACR2a-expressing Jurkat cells were allowed to settle on anti-CD3–coated glass and were either not treated or treated with 2 µM LatA for 5 min to depolymerize actin. Kymographs are derived from the yellow dashed lines indicated on the images. Scale bar: 10 µm. **(B)** Velocities of the CRACR2a cortical puncta and actin retrograde flow. Velocities are quantified based on at least 50 kymograph traces from eight cells in each condition. Data are mean ± SD.

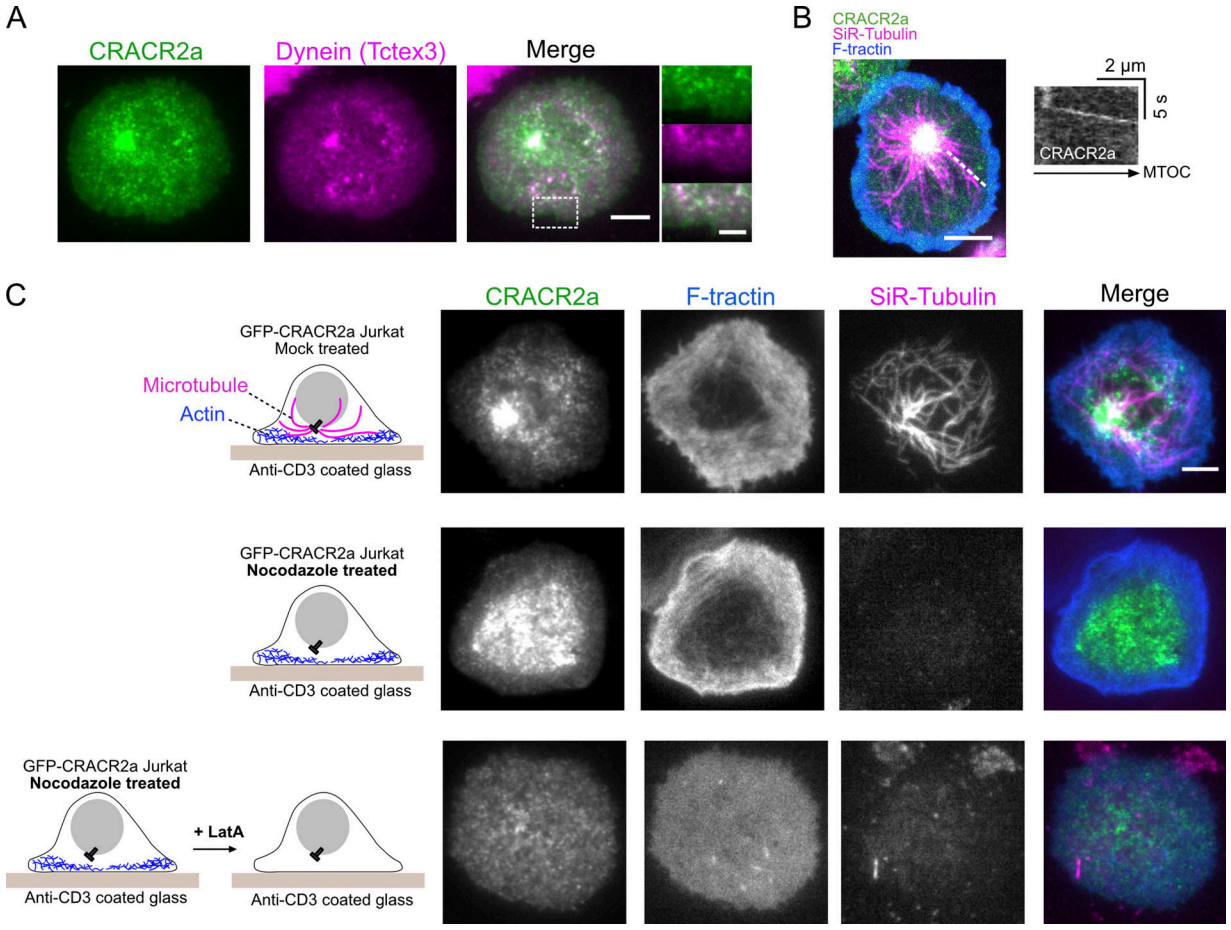

Figure 7. **CRACR2a cortical puncta recruit dynein to detach from the actin cortex and travel to the MTOC. (A)** Colocalization between CRACR2a cortical puncta and dynein (visualized by mCherry-Tctex3, a dynein light chain). Scale bar: 5 µm. Inset scale bar: 2 µm. **(B)** Imaging CRACR2a cortical puncta dynamics on actin (visualized by mCherry-F-tractin) and microtubules (visualized by SiR-Tubulin) using a spinning disk confocal microscope. Kymograph analysis along the indicated line is shown on the right. In total, 28 cells were imaged continuously for 50 s each, and 16 events of a cortical punctum moving on a microtubule were observed. Scale bar: 5 µm. **(C)** Changes in CRACR2a cortical puncta dynamics in response to cytoskeleton disassembly by nocodazole (5 µM) and/or latrunculin A (2 µM). The cells are treated as indicated by the diagrams shown on the left side. Scale bar: 5 µm.

CRACR2a is involved in endosomal trafficking of CD47

The formation of CRACR2a cortical puncta at the plasma membrane and their microtubule-dependent movement away from the cortex and toward the cell interior suggests that CRACR2a might be involved in endocytosis. We sought to identify cell surface proteins that undergo endocytosis and colocalize with the CRACR2a vesicular compartment inside the cell. We selected a set of candidate molecules, with distinct membrane topologies, that have been shown previously to be internalized through various endocytic pathways (Maldonado-Báez et al., 2013; Boucrot et al., 2015; Table 1). We employed an antibody/ligand internalization assay to examine the endocytosis of cell surface molecules. Briefly, endocytosis was suppressed by incubating cells on ice, and cell surface proteins were labeled on the extracellular side using fluorescent-conjugated antibodies or ligand. Excess labeling antibodies/ligands were then removed. Cells were warmed to 37°C rapidly and stimulated with immobilized anti-CD3 antibodies to promote endocytosis and transport to the MTOC. The amount of internalized antibody or ligand within the CRACR2a compartment was determined by confocal imaging. Among the candidates tested, only the multipass transmembrane protein CD47 was strongly internalized into the CRACR2a compartment at the MTOC (Fig. 8, A and B). Confocal z-sections of the cells confirmed that the cell surface–labeled CD47 was indeed internalized into the interior of the cell (Fig. S5). Stimulation of Jurkat cells with ionomycin alone also promoted internalization of CD47 into the CRACR2a compartment (Fig. 8, C and D).

We further examined the internalization of CD47 in wild-type Jurkat T cells or in the CRACR2a knockout cell line, J.CRACR2a. Qualitatively, antibody-labeled CD47 could still be observed within endocytic vesicles in J.CRACR2a (Fig. 8 E). This could be due to the presence of CRACR2a-independent endocytic pathways that also mediate the internalization of CD47. We therefore quantified the amount of internalized CD47 transported to within 2.5 µm of the MTOC, the region where the majority of the CRACR2a vesicular compartments concentrate (Fig. 3 A). Deletion of CRACR2a significantly reduced the amount of CD47 within this region (Fig. 8 E), which could result from a reduction in CD47 endocytosis and/or retrograde transport of

Table 1. **Candidate cell surface proteins tested for internalization into CRACR2a vesicular compartment**

	Transferrin receptor	TCR	CD47	CD59	CD147
Type	Type II single transmembrane protein (dimer)	Multichain receptor complex	Five-pass transmembrane protein	GPI-anchored cell surface protein	Type I single transmembrane protein
Endocytic pathway	CME	CME and CIE	CIE?[a]	CIE	CIE

CIE, clathrin-independent endocytosis; CME, clathrin-mediated endocytosis.
[a]Listed as CIE cargo in Boucrot et al. (2015), but no primary data could be found.

CD47-positive endosomes after internalization. Taking these results together, we propose that CRACR2a is involved in a form of calcium-stimulated endocytic process, and that CD47 is one of the cargoes transported through this pathway.

Discussion

In this study, we provide evidence that the Rab GTPases CRACR2a and Rab45 are unusual adaptor proteins that activate dynein–dynactin motility. Several Rab GTPases have been shown to bind directly to dynein adaptor proteins. Rab6, for example, binds to the C-terminal coiled-coil of the adaptor BicD, which then uses its N-terminal coiled-coil to engage dynein–dynactin (Matanis et al., 2002; Urnavicius et al., 2015; Huynh and Vale, 2017). Rab11FIP3 has an N-terminal EF-hands and a coiled-coil for dynein activation, while containing a C-terminal Rab11-binding domain (Horgan et al., 2010; McKenney et al., 2014). In these examples, the Rab binding domains themselves do not appear to contribute directly to binding of dynein–dynactin; instead they mainly act to recruit the adaptors to specific membrane cargoes (Reck-Peterson et al., 2018). Our evidence indicates that CRACR2a and Rab45 represent gene fusions of a

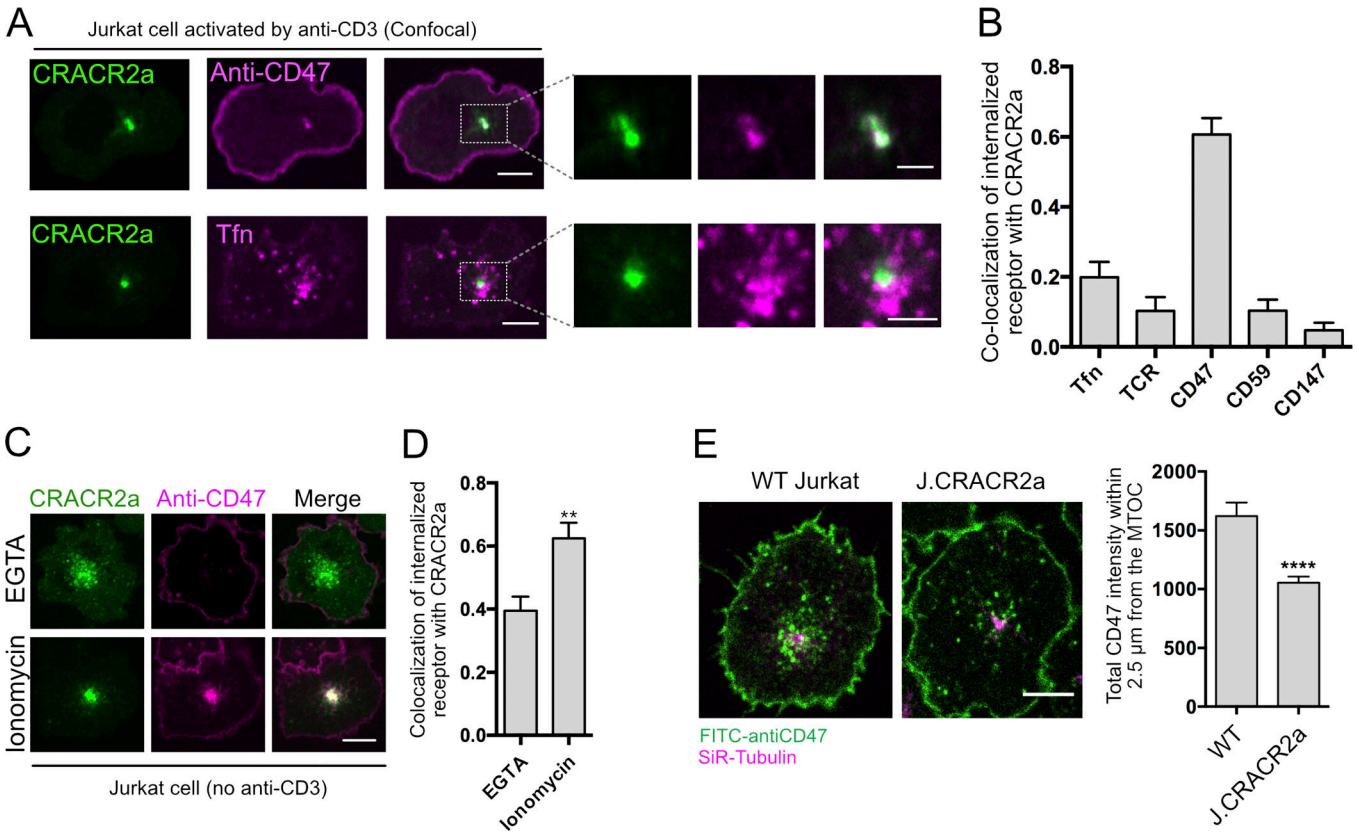

Figure 8. **CRACR2a is involved in endosomal trafficking of CD47. (A)** CD47 but not Transferin (Tfn) is internalized into CRACR2a compartment at the MTOC. Scale bar: 5 µm. Inset scale bar: 2 µm. **(B)** Quantification of the fraction of internalized receptor that colocalizes with the CRACR2a compartment. Data are from at least 18 cells collected during three independent experiments. Errors bar indicate SEM.**(C)** Ionomycin stimulates CD47 internalization into CRACR2a compartment. Scale bar: 10 µm. **(D)** Quantifications of the fraction of internalized CD47 in CRACR2a compartment in EGTA or ionomycin condition. Data are from at least 20 cells collected during three independent experiments. Error bar indicates SEM. **, P < 0.01, Student's *t* test. **(E)** Deletion of CRACR2a reduced the amount of CD47 internalized into MTOC proximal region (<2.5 µm). Scale bar: 5 µm. Data are from at least 149 cells collected during three independent experiments. Error bar indicates SEM. ****, P < 0.0001, Student's *t* test.

coiled-coil dynein adaptor with a Rab GTPase. We also demonstrate that the dynein adaptor function of CRACR2a is regulated by calcium in vitro, and that calcium release accompanying Jurkat T cell activation results in up-regulation of CRACR2a–dynein–mediated trafficking. We further found that CRACR2a forms diffraction-limited cortical puncta at the IS of activated Jurkat cells. We showed that CRACR2a cortical puncta require microtubules to detach from the cell cortex and travel to the MTOC, suggesting that they are involved in an endocytic transport process.

CRACR2a is a calcium-regulated dynein adaptor protein

Rab45 and CRACR2a, together with Rab11FIP3 and the Ninein family, constitute a group of adaptor proteins that contain EF-hands and coiled-coil domains. Recent structural studies have demonstrated that the coiled-coil domains play crucial roles in bridging the interaction between dynein and dynactin (Urnavicius et al., 2015, 2018; Zhang et al., 2017). In contrast, the role of the EF-hands in these proteins is less clear. Domains outside of the coiled-coil region in adaptor proteins could facilitate or regulate their interactions with dynein–dynactin. The Hook domain of Hook3, for example, directly binds to the dynein light-intermediate chain (Zhang et al., 2014; Schroeder and Vale, 2016). It is possible that the EF-hands in Rab45 and CRACR2a play a similar role. Moreover, EF-hands can assume different conformations depending on their calcium binding state (Yap et al., 1999). Interactions between EF-hands and their binding partners are therefore often calcium regulated (Lewit-Bentley and Réty, 2000). Our study establishes CRACR2a as the first dynein adaptor protein that responds to calcium changes in vitro and in cells and shows that the EF-hands are required for this regulation. CRACR2a, therefore, can serve to connect calcium signaling to the regulation of dynein function. We demonstrate that CRACR2a's calcium regulation couples T cell activation to dynein-dependent intracellular transport.

The CRACR2a vesicular compartment and its function in T cells

Our data suggest that the intracellular CRACR2a vesicular compartment, at least in part, is derived through an endocytic process. Evidence in support of this hypothesis is the observation that cell surface CD47 pulse labeled with a fluorescent antibody colocalized with GFP-CRACR2a after internalization. Consistent with Srikanth et al. (2016), we found that the CRACR2a vesicular compartment moves toward the IS during Jurkat cell activation, likely due to the repositioning of the MTOC and the associated endomembrane system (Stinchcombe and Griffiths, 2014). Srikanth et al. (2016) further showed that GFP-CRACR2a in resting Jurkat cells partially overlaps with the Rab8-positive trans-Golgi network. However, we find that only CRACR2a, but neither Rab8A nor Rab11A, responds to ionomycin-induced calcium increase by further clustering at the MTOC, suggesting that the CRACR2a intracellular vesicular compartment is distinct from well-characterized endosomal compartments. The role of CRACR2a and the calcium-induced translocation of CD47 endosomes to the MTOC in T cell function remains a topic for future exploration.

A possible role of CRACR2A, microtubules, and dynein in endocytosis at the T cell IS

In addition to the intracellular vesicular compartment containing CRACR2A, we observed that CRACR2a forms numerous cortical puncta, which are dim and diffraction-limited dots at the cell membrane. The cortical puncta emerge initially from the lamella edge of the cell and migrate centripetally with actin retrograde flow (Fig. 6 and Video 3). These puncta are distinct from the larger CRACR2a vesicles reported by Srikanth et al. (2016) that occasionally could be observed to enter into the TIRF view in the central region of the synapse and move bidirectionally. Although the exact nature of the CRACR2a cortical puncta remains unclear, we find that they form through an actin-dependent process at the periphery of the cell and are visible only within the TIRF illumination zone (<200 nm). These results suggest that they are localized at the plasma membrane or the adjacent actin cortex.

We also show that CRACR2a cortical puncta recruit dynein when they form. We observed discrete events in which these cortical puncta transitioned from slow actin-mediated retrograde flow to fast microtubule-based movement toward the MTOC. If microtubules are depolymerized, then CRACR2a cortical puncta appear not to be internalized and instead form a disk at the central region of the IS, accumulating there through actin retrograde flow. From these observations, we infer that CRACR2a cortical puncta are first nucleated at the plasma membrane and then become internalized through an endocytosis process.

Collectively, these observations suggest a role of dynein–dynactin and microtubules in some early steps of CRACR2a-associated endocytosis (Fig. 9), either in mechanical pulling that aids in the formation of the endosomal vesicle itself (Day et al., 2015; Simunovic et al., 2017) or in extracting the vesicle from the actin-rich cortex and delivering it to the cell interior. In contrast to the studies documenting involvement of actin in endosome formation (Mayor et al., 2014; Ferreira and Boucrot, 2017), a role for microtubules in early events of endocytosis is less well established. An earlier study showed that inhibition of dynein function or disruption of microtubules suppresses a form of chorea toxin–induced tubular endosome formation (Day et al., 2015). This study speculated that a pulling force generated by dynein might promote the membrane invagination required for endocytosis, although it was not investigated whether dynein localizes to these tubular invaginations. Our data suggest that the CRACR2a cortical puncta eventually mature into endocytic vesicles, and that dynein and a specific dynein adapter (CRACR2a) are involved in extracting these vesicles from the actin cortex and delivering them to the cell interior. More detail on the role that dynein plays in this form of endocytosis awaits further studies. However, CRACR2a should provide a useful tool to tease apart this very specific role of dynein in endocytosis.

Materials and methods

DNA constructs, antibodies, and chemical inhibitors

The cDNA for human Rab45 (NM_152573.3) and CRACR2a (NM_001144958.1) was synthesized by Genscript. Detailed information

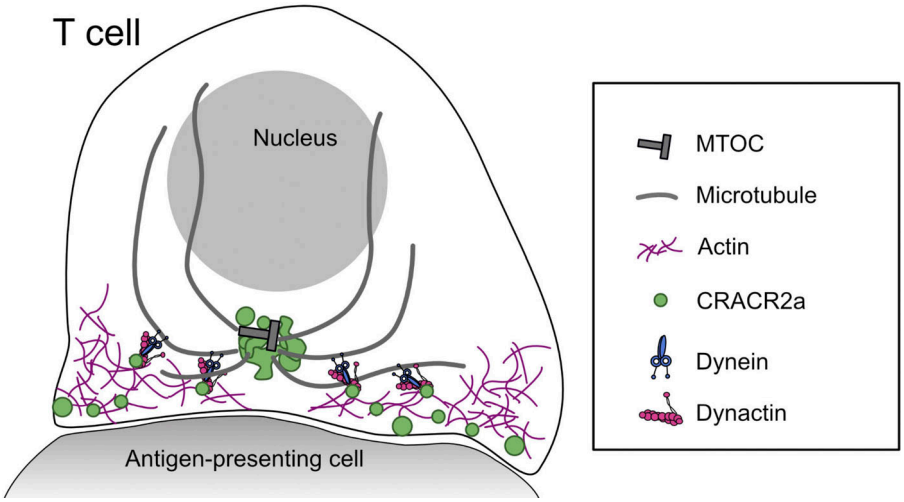

Figure 9. **A schematic of CRACR2a–dynein–mediated endocytosis during T cell activation.** Activation of a T cell by an antigen presenting cell causes increase of intracellular calcium, which promotes the formation of CRACR2a cortical puncta at the IS. Activation of dynein–dynactin by CRACR2a facilitates the detachment of the cortical puncta from the actin cortex and initiates microtubule minus-end–directed transport.

about the various DNA constructs, antibodies, and inhibitors used can be found in Table S1.

Protein purification

Rab45 and CRACR2a expressed in bacteria are prone to degradation. To enrich for full-length proteins, we adopted a tandem affinity purification strategy. Briefly, Rab45 and CRACR2a constructs in pET28 vectors were transformed into the *Escherichia coli* strain BL21 RIPL (Agilent). Bacterial culture was grown in Terrific Broth at 37°C until growth reached ∼2.0 OD_{600}. The temperature was then lowered to 18°C, and the culture was induced overnight with 0.5 mM IPTG. Bacterial pellets were resuspended in Ni-A buffer (50 mM Tris-HCl, pH 8.0, 500 mM NaCl, 2 mM $MgCl_2$, 5% glycerol, 10 mM imidazole, and 3 mM 2-mercaptoethanol). Cells were lysed using an Emulsiflex press (Avestin) and clarified at 18,000 rpm using a Sorvall SS-34 rotor for 60 min at 4°C. Lysates were filtered through a 0.45-µm filter before loading to a HisTrap FF column (GE Healthcare). The column was then washed with 20 column volumes (CV) of Ni-A buffer. Bound protein was eluted with 10 CV Ni-B buffer (20 mM Tris-HCl, pH 8.0, 300 mM NaCl, 5% glycerol, 500 mM imidazole, and 3 mM 2-mercaptoethanol). Eluate was then directly loaded to a StrepTrap HP column (GE Healthcare). The column was washed with 20 CV wash buffer (20 mM Tris-HCl, pH 8.0, 300 mM NaCl, 2 mM $MgCl_2$, 5% glycerol, and 2 mM DTT), and the bound protein was eluted with 10 CV elution buffer (20 mM Tris-HCl, pH 8.0, 300 mM NaCl, 2 mM $MgCl_2$, 5% glycerol, 3 mM desthiobiotin, and 2 mM DTT). Eluted proteins were further purified with a Superose 6 10/300GL (GE Healthcare) gel filtration column. Peak fractions were pooled and concentrated and then flash frozen in liquid nitrogen. Dynein and dynactin were prepared from RPE-1 cells as previously described (Huynh and Vale, 2017).

EGTA buffered calcium solution

To maintain free calcium concentration at physiologically relevant levels (100 nM to ∼10 µM), it is essential to use an EGTA:Ca^{2+} buffer system, which is prepared by mixing EGTA and $CaCl_2$ at a calculated ratio to achieve the desired free calcium concentration (Bers et al., 2010). We followed the protocol described by Bers et al. (2010) and used the Maxchelator tool that the authors developed (https://somapp.ucdmc.ucdavis.edu/pharmacology/bers/maxchelator/CaMgATPEGTA-NIST-Plot.htm) to calculate the ratio of EGTA and $CaCl_2$ needed to maintain the desired calcium concentration. The following parameters were used for the calculation: temperature 25°C, pH 7.3, ionic 0.04 N, 1 mM ATP, and 2 mM Mg^{2+}.

Dynein–dynactin pulldown assay

Pulldown of dynein/dynactin was performed as previously described (Huynh and Vale, 2017). Briefly, dynein/dynactin isolated from RPE1 cells were mixed with 20 nM purified Rab45 or CRACR2a and 15 µl preequilibrated Streptactin Sepharose beads (GE Healthcare) in 300 µl binding buffer (50 mM Hepes, pH 7.4, 20 mM NaCl, 1 mM Mg-Acetate, 10% glycerol, 0.1% NP-40, and 2 mM DTT). The mixture was incubated at 4°C for 1 h. Beads were pelleted at 1,000× relative centrifugal force for 2 min and washed four times with 500 µl binding buffer. The proteins were eluted by boiling in SDS loading buffer for 5 min and loaded onto SDS-PAGE gel. The amounts of CRACR2a and Rab45 in the pulldown samples were visualized by Coomassie staining. The amounts of dynein and dynactin were detected via Western blot with antibodies against dynein heavy chain and the p150 subunit of dynactin, respectively. In the pulldown assay shown in Fig. 2 A, 2 mM EGTA or EGTA:Ca^{2+} was added to the binding buffer to deplete calcium or to maintain a free calcium concentration of 2 µM. Information about antibodies used can be found in Table S1.

Single-molecule motility assay

Microtubules were prepared as previously described (Huynh and Vale, 2017). Briefly, unlabeled tubulin, biotinylated tubulin, and Alexa Fluor 640–labeled tubulin were mixed at a ratio of ∼5:1:1 in BRB80 (80 mM Pipes, pH 6.8, 1 mM EGTA, and 1 mM $MgCl_2$). GTP was added to 5 mM final concentration, and the mixture was incubated at 37°C for 10 min. Taxol was then added to 20 µM, and microtubules were allowed to polymerize overnight. Before use, microtubules were spun over a 25% sucrose

cushion in BRB80 with 10 µM taxol at 20,000 *g* for 10 min and resuspended in BRB80 with 10 µM taxol but without EGTA.

For in vitro motility assays, purified Rab45 or CRACR2a was mixed with dynein–dynactin at a 5:1 ratio in a 25-µl reaction volume in assay buffer (50 mM Hepes, pH 7.4, 2 mM magnesium acetate, 10% glycerol, and 2 mM DTT) along with 0.1 mg/ml biotin-BSA, 0.5% pluronic acid F-127, and 0.2 mg/ml κ-casein. In the motility assay shown in Fig. 2 B, EGTA:Ca^{2+} buffer (1 mM EGTA and varying concentrations of $CaCl_2$) was added to the assay buffer to maintain the desired free calcium concentration. The mixture was incubated on ice for at least 1 h. Flow chambers with attached microtubules were prepared as described (Schroeder and Vale, 2016). The dynein–dynactin adaptor complex was then added in the presence of 2 mM ATP and the Trolox/PCD oxygen scavenging system (Aitken et al., 2008). TIRF imaging of single molecules was performed on a Nikon Eclipse TE200-E microscope equipped with an Andor iXon EM CCD camera, a 100× 1.49-NA objective, and MicroManager software (Edelstein et al., 2014). Exposure conditions were 200 ms per frame with 1-s interval for 150 frames. Kymographs were created for randomly selected microtubules using Fiji (Schindelin et al., 2012), and the number of processive particles was counted manually.

Cell culture and transduction

U2OS cells and HEK293T cells were cultured in DMEM containing 10% FBS and penicillin/streptomycin/L-glutamine. Jurkat cells were cultured in RPMI 1640 containing 10% FBS and penicillin/streptomycin/L-glutamine. Lentiviral transduction was used to create cell lines stably expressing GFP-CRACR2a, and GFP-positive cells were selected by FACS. Transient transfection of Jurkat cells was performed with TransIT-Jurkat (Mirus Bio) following the manufacturer's protocol.

Peroxisome assay

Unlike other dynein adaptors, Rab45 and CRACR2a contain a Rab GTPase domain that associates with intracellular membranes through its C-terminal geranylgeranylation. To prevent concurrent localization of Rab45 and CRACR2a to peroxisomes and nonperoxisomal membrane compartments, which would complicate the analysis, we deleted their C-terminal CCX prenylation motifs and cloned them into the pmCherry-FKBP plasmid. The assay was performed as previously described (Huynh and Vale, 2017). Briefly, U2OS cells were cotransfected with mCherry-adaptor-FKBP and PEX-GFP-FRB plasmids. 24 h after transfection, cells were treated with 0.25 µM rapamycin for 50 min, and for the last 10 min, cells were stained with CellMask DeepRed. After washing with PBS twice, cells were fixed with 4% PFA for 15 min at room temperature. Images were acquired on a Nikon Eclipse TE200-E spinning disk confocal microscope equipped with an Andor iXon EM CCD camera, a 40× 0.95-NA objective, and MicroManager software (Edelstein et al., 2014). We manually quantified the number of cells exhibiting a clustered peroxisome phenotype, which is defined as all of the peroxisome signal in the GFP channel coalescing into a cluster at the cell center as shown in Fig. 1 F.

Generation of CRACR2a knockout Jurkat cell line using CRISPR/Cas9

The CRACR2a knockout Jurkat cell line, J.CRACR2a, was generated by transiently expressing Cas9 and a single guide (sgRNA; 5′-ACAGCAGAGGGATTCTTAGG-3′) against the CRACR2A exon 8. In brief, the sgRNA was cloned into the pU6-(BbsI)_CBh-Cas9-T2A-BFP vector (Addgene; plasmid no. 64323) and electroporated into Jurkat cells. Single cells were sorted into 96-well plates the next day, and monoclonal cell lines were replated to six-well plates. Successful knockout clones were selected by screening with immunoblots probed for anti-CRACR2A. Genomic DNA of the J.CRACR2a was purified and used as a template for genotyping. PCR products amplified covering the sgRNA cutting site were TOPO cloned into pCR2.1 vectors and sequenced to verify that the genome editing generated premature stop codons in all the alleles.

T cell activation and calcium stimulation

Glass-bottom 96-well plates (MatriCal) were coated with anti-CD3ε antibody (clone OKT3) or with IgG isotype control at room temperature for 2–4 h or at 4°C overnight. In Fig. 8 A, to monitor TCR internalization, cells were activated by a different anti-CD3 antibody (clone UCHT1), which does not compete with the Alexa Fluor 647–conjugated antibody used for labeling TCR. Wells were washed once with PBS. Jurkat T cells were resuspended in RPMI 1640 (no phenol red, with 25 mM Hepes, pH 7.4) and rested for 30 min before being dropped onto antibody-coated wells. For ionomycin stimulation, Jurkat cells were resuspended in HBSS with 25 mM Hepes, pH 7.4, and added to wells. Cells were allowed to settle for 15 min, and then ionomycin and $CaCl_2$ were added to final concentrations of 0.5 µM and 1 mM, respectively.

Confocal imaging of CRACR2a cortical puncta and vesicular compartments

Jurkat cells expressing GFP-CRACR2a were stimulated as described above. For SiR-Tubulin staining, cells were stained with 100 nM SiR-Tubulin in their growth medium for 4 h at 37°C. Cells were imaged on a Nikon Eclipse TE200-E spinning disk confocal microscope equipped with an Andor iXon EM CCD camera, a 100× 1.49-NA oil objective, and MicroManager software (Edelstein et al., 2014). To calculate the relative enrichment of the CRACR2a compartment at the MTOC, a series of z-sections at 0.3-µm z-intervals was taken. The location of the MTOC was identified through the SiR-Tubulin channel. The MTOC enrichment was quantified using Fiji by measuring the mean intensity of GFP signal within 0.5 µm radius of the MTOC, which was then normalized by the mean intensity of GFP in the 0.5–2.5-µm range around the MTOC. In Fig. 7 B, cells expressing mCherry-F-tractin and GFP-CRACR2a were labeled with 100 nM SiR-Tubulin for 4 h. A single frame of F-tractin and SiR-Tubulin was acquired, and the cells were then imaged continuously using a 488-nm laser at 6.7 frames/s acquisition rate.

TIRF imaging of CRACR2a cortical puncta at the IS

Jurkat cells expressing GFP-CRACR2a were stimulated as described above. TIRF imaging was performed on a Nikon Eclipse

TE200-E microscope equipped with a motorized TIRF arm, a Hamamatsu Flash 4 camera, a 100× 1.49-NA oil objective, and MicroManager software (Edelstein et al., 2014). We found that the GFP-CRACR2a cortical puncta have a very low signal-to-noise ratio, possibly due to a high level of diffusive GFP signal present at the cell membrane. We used relatively low laser power and long exposure time (800 ms) with 2–4-s imaging interval to improve the signal-to-noise ratio and reduce photobleaching. To quantify the number of CRACR2a puncta formed, we used the ImageJ plug-in Spot Counter (http://imagej.net/SpotCounter) with BoxSize set to 3 and Noise tolerance set to 100. The number of detected spots was quantified over 20 frames, and the average number of spots per frame per square micrometer was calculated. One or two regions of interest (ROIs) at the periphery of the cell were selected for quantification. For data shown in Fig. 5 B, chemical inhibitors (see Table S1 for concentrations used) were added, and cells were treated for 5 min before being imaged using TIRF. For K44A dominant-negative dynamin data in Fig. 5 B, K44A Dyn1-mRFP plasmid was transfected into GFP-CRACR2a–expressing Jurkat cells, and the number of CRACR2a cortical puncta in mRFP-positive cells was determined as above. For the nocodazole-treated cell shown in Fig. 7 C, Jurkat cells were treated with 5 µM nocodazole for 30 min in RPMI 1640 before being added to antibody-coated wells. Further treatments with latrunculin A (LatA) were performed by adding 2 µM final concentration of LatA to the well and incubating for 5 min. Detailed information regarding inhibitors and concentrations used can be found in Table S1.

Antibody internalization assay

For data shown in Fig. 8 (A and B), GFP-CRACR2a Jurkat cells were washed once with RPMI 1640 (no phenol red, with 25 mM Hepes, pH 7.4) to remove serum. Cells were then incubated on ice for 10 min to inhibit endocytosis, before staining with Alexa Fluor 647–labeled antibodies or transferrin for 20 min on ice. Cells were then washed twice with cold RPMI 1640 before being added to anti-CD3–coated wells with prewarmed RPMI 1640. 25–30 min after addition of the cells to the wells, z-sections were acquired using a spinning disk confocal microscope at 0.3-µm z-interval. For data shown in Fig. 8 C, cells were stained with Alexa Fluor 647–conjugated anti-CD47 as described above, except 1 mM EGTA was added to deplete calcium from the medium. Cells were allowed to settle on noncoated glass for 20 min, and confocal z-sections were acquired. Cells were then treated with 0.5 µM ionomycin and 2 mM $CaCl_2$ for 15 min, and confocal z-sections were taken. The JACoP plug-in for Fiji was used for quantifications of the colocalization of internalized receptor in CRACR2a compartments (Bolte and Cordelières, 2006). A representative z-section was selected and an ROI was manually drawn to exclude cell membrane. After background subtraction using thresholding, the colocalization was calculated using the M1 and M2 coefficients analysis. We defined the GFP-CRACR2a channel as channel A and the Alexa Fluor 647 channel as channel B. The M2 coefficient was calculated as follows (Bolte and Cordelières, 2006):

$$M_2 = \frac{\sum_i B_{i,coloc}}{\sum_i B_i}.$$

B_i is the intensity of pixel i in channel B; A_i is the intensity of pixel i in channel A; $B_{i,\ coloc} = B_i$ if $A_i > 0$; $B_{i,\ coloc} = 0$ if $A_i = 0$.

In this experiment, the M2 coefficient represents the amount of internalized receptor within the CRACR2a compartment normalized by the total amount of internalized receptor.

Quantification of CD47 internalization in wild-type and J.CRACR2a Jurkat cells

For data shown in Fig. 8 E, parental or CRACR2a knockout Jurkat cells were stained with 100 nM SiR-Tubulin for 4 h in growth medium and washed once with RPMI 1640 (no phenol red, with 25 mM Hepes, pH 7.4) to remove serum. Cells were then incubated on ice for 10 min to inhibit endocytosis, before staining with FITC-labeled anti-CD47 antibody for 20 min on ice. Cells were washed once and then incubated at 37°C in RPMI 1640 with 0.5 µM ionomycin and 1 mM $CaCl_2$ to stimulate CD47 internalization. To reduce the amount of FITC signal at the cell surface, which causes high background signal, 0.2% Trypan blue was added to quench FITC exposed at the cell surface. z-Sections were acquired using a spinning disk confocal microscope at 0.3-µm z-interval. Image background was determined by measuring mean intensity in an ROI outside of cells. After background subtraction, quantification of internalized CD47 was performed by measuring the amount of total FITC signal within a 2.5-µm circle around the MTOC.

Online supplemental material

Fig. S1 shows SDS gels of purified recombinant proteins and the effect of calcium or EGTA on the motility of dynein–dynactin-Rab45. Fig. S2 shows the Western blot of CRACR2a in different cell lines used in the study. Fig. S3 shows SiR-Tubulin staining of microtubules as well as translocation of CRACR2a vesicular compartment toward the IS. Fig. S4 shows the effects of calcium on subcellular distributions of CRACR2a, Rab8A, and Rab11A. Fig. S5 shows confocal z-sections of CRACR2a and internalized anti-CD47. Video 1 shows confocal time-lapse imaging of GFP-CRACR2a intracellular compartments in Jurkat T cells. Video 2 shows the dynamics of CRACR2a cortical puncta at the T cell IS. Video 3 shows that CRACR2a cortical puncta migrate with actin retrograde flow. Video 4 shows that latrunculin treatment disrupts the retrograde movement of CRACR2a cortical puncta. Video 5 shows that dynein is recruited to CRACR2a puncta. Video 6 shows that nocodazole treatment causes accumulation of CRACR2a cortical puncta at the central region of the IS. Table S1 contains detailed information about the various DNA constructs, antibodies, and inhibitors used.

Acknowledgments

We thank N. Stuurman for help with microscopy and image analysis. We also thank the Vale laboratory members for help with reagents and critiques of the manuscript.

This work was funded by the National Institutes of Health (5R35GM118106-02, R.D. Vale; 1R37AI114575, A. Weiss; and 5R37AI114575, W. Lu) and the Howard Hughes Medical Institute (R.D. Vale and A. Weiss).

The authors declare no competing financial interests.

Author Contributions: Y. Wang and R.D. Vale conceived the study and designed the experiments. W. Huynh and T.D. Skokan performed the peroxisome assays and initial biochemical purifications and analyzed the data. W. Lu generated the CRACR2a knockout Jurkat cell line. Y. Wang performed all other experiments and analyzed the data. Y. Wang and R.D. Vale wrote the manuscript, and all co-authors provided feedback.

Submitted: 14 June 2018
Revised: 14 December 2018
Accepted: 7 February 2019

References

Aitken, C.E., R.A. Marshall, and J.D. Puglisi. 2008. An oxygen scavenging system for improvement of dye stability in single-molecule fluorescence experiments. *Biophys. J.* 94:1826–1835. https://doi.org/10.1529/biophysj.107.117689

Bers, D.M., C.W. Patton, and R. Nuccitelli. 2010. A Practical Guide to the Preparation of Ca2+ Buffers. *In Methods in Cell Biology*. M. Whitaker, editor. Academic Press, Cambridge, MA; 1–26.

Bolte, S., and F.P. Cordelières. 2006. A guided tour into subcellular colocalization analysis in light microscopy. *J. Microsc.* 224:213–232. https://doi.org/10.1111/j.1365-2818.2006.01706.x

Boucrot, E., A.P.A. Ferreira, L. Almeida-Souza, S. Debard, Y. Vallis, G. Howard, L. Bertot, N. Sauvonnet, and H.T. McMahon. 2015. Endophilin marks and controls a clathrin-independent endocytic pathway. *Nature.* 517:460–465. https://doi.org/10.1038/nature14067

Day, C.A., N.W. Baetz, C.A. Copeland, L.J. Kraft, B. Han, A. Tiwari, K.R. Drake, H. De Luca, D.J.-F. Chinnapen, M.W. Davidson, et al. 2015. Microtubule motors power plasma membrane tubulation in clathrin-independent endocytosis. *Traffic.* 16:572–590. https://doi.org/10.1111/tra.12269

Doherty, G.J., and H.T. McMahon. 2009. Mechanisms of endocytosis. *Annu. Rev. Biochem.* 78:857–902. https://doi.org/10.1146/annurev.biochem.78.081307.110540

Dustin, M.L., A.K. Chakraborty, and A.S. Shaw. 2010. Understanding the structure and function of the immunological synapse. *Cold Spring Harb. Perspect. Biol.* 2:a002311. https://doi.org/10.1101/cshperspect.a002311

Edelstein, A.D., M.A. Tsuchida, N. Amodaj, H. Pinkard, R.D. Vale, and N. Stuurman. 2014. Advanced methods of microscope control using μManager software. *J. Biol. Methods.* 1:e10. https://doi.org/10.14440/jbm.2014.36

Ferreira, A.P.A., and E. Boucrot. 2017. Mechanisms of Carrier Formation during Clathrin-Independent Endocytosis. *Trends Cell Biol.* 28:188–200. https://doi.org/10.1016/j.tcb.2017.11.004

Hirokawa, N., Y. Noda, Y. Tanaka, and S. Niwa. 2009. Kinesin superfamily motor proteins and intracellular transport. *Nat. Rev. Mol. Cell Biol.* 10:682–696. https://doi.org/10.1038/nrm2774

Hoogenraad, C.C., P. Wulf, N. Schiefermeier, T. Stepanova, N. Galjart, J.V. Small, F. Grosveld, C.I. de Zeeuw, and A. Akhmanova. 2003. Bicaudal D induces selective dynein-mediated microtubule minus end-directed transport. *EMBO J.* 22:6004–6015. https://doi.org/10.1093/emboj/cdg592

Horgan, C.P., S.R. Hanscom, R.S. Jolly, C.E. Futter, and M.W. McCaffrey. 2010. Rab11-FIP3 links the Rab11 GTPase and cytoplasmic dynein to mediate transport to the endosomal-recycling compartment. *J. Cell Sci.* 123:181–191. https://doi.org/10.1242/jcs.052670

Hutagalung, A.H., and P.J. Novick. 2011. Role of Rab GTPases in membrane traffic and cell physiology. *Physiol. Rev.* 91:119–149. https://doi.org/10.1152/physrev.00059.2009

Huynh, W., and R.D. Vale. 2017. Disease-associated mutations in human BICD2 hyperactivate motility of dynein–dynactin. *J. Cell Biol.* 216:3051–3060. https://doi.org/10.1083/jcb.201703201

Johnson, D.L., J. Wayt, J.M. Wilson, and J.G. Donaldson. 2017. Arf6 and Rab22 mediate T cell conjugate formation by regulating clathrin-independent endosomal membrane trafficking. *J. Cell Sci.* 130:2405–2415. https://doi.org/10.1242/jcs.200477

Kapitein, L.C., M.A. Schlager, W.A. van der Zwan, P.S. Wulf, N. Keijzer, and C.C. Hoogenraad. 2010. Probing intracellular motor protein activity using an inducible cargo trafficking assay. *Biophys. J.* 99:2143–2152. https://doi.org/10.1016/j.bpj.2010.07.055

Lewit-Bentley, A., and S. Réty. 2000. EF-hand calcium-binding proteins. *Curr. Opin. Struct. Biol.* 10:637–643. https://doi.org/10.1016/S0959-440X(00)00142-1

Liu, Y., H.K. Salter, A.N. Holding, C.M. Johnson, E. Stephens, P.J. Lukavsky, J. Walshaw, and S.L. Bullock. 2013. Bicaudal-D uses a parallel, homodimeric coiled coil with heterotypic registry to coordinate recruitment of cargos to dynein. *Genes Dev.* 27:1233–1246. https://doi.org/10.1101/gad.212381.112

Maldonado-Báez, L., C. Williamson, and J.G. Donaldson. 2013. Clathrin-independent endocytosis: a cargo-centric view. *Exp. Cell Res.* 319:2759–2769. https://doi.org/10.1016/j.yexcr.2013.08.008

Matanis, T., A. Akhmanova, P. Wulf, E. Del Nery, T. Weide, T. Stepanova, N. Galjart, F. Grosveld, B. Goud, C.I. De Zeeuw, et al. 2002. Bicaudal-D regulates COPI-independent Golgi-ER transport by recruiting the dynein-dynactin motor complex. *Nat. Cell Biol.* 4:986–992. https://doi.org/10.1038/ncb891

Mayor, S., R.G. Parton, and J.G. Donaldson. 2014. Clathrin-independent pathways of endocytosis. *Cold Spring Harb. Perspect. Biol.* 6:a016758. https://doi.org/10.1101/cshperspect.a016758

McKenney, R.J., W. Huynh, M.E. Tanenbaum, G. Bhabha, and R.D. Vale. 2014. Activation of cytoplasmic dynein motility by dynactin-cargo adapter complexes. *Science.* 345:337–341. https://doi.org/10.1126/science.1254198

Miller, S.G., L. Carnell, and H.H. Moore. 1992. Post-Golgi membrane traffic: brefeldin A inhibits export from distal Golgi compartments to the cell surface but not recycling. *J. Cell Biol.* 118:267–283. https://doi.org/10.1083/jcb.118.2.267

Reck-Peterson, S.L., W.B. Redwine, R.D. Vale, and A.P. Carter. 2018. The cytoplasmic dynein transport machinery and its many cargoes. *Nat. Rev. Mol. Cell Biol.* 19:382–398. https://doi.org/10.1038/s41580-018-0004-3

Redwine, W.B., M.E. DeSantis, I. Hollyer, Z.M. Htet, P.T. Tran, S.K. Swanson, L. Florens, M.P. Washburn, and S.L. Reck-Peterson. 2017. The human cytoplasmic dynein interactome reveals novel activators of motility. *eLife.* 6:e28257. https://doi.org/10.7554/eLife.28257

Schindelin, J., I. Arganda-Carreras, E. Frise, V. Kaynig, M. Longair, T. Pietzsch, S. Preibisch, C. Rueden, S. Saalfeld, B. Schmid, et al. 2012. Fiji: an open-source platform for biological-image analysis. *Nat. Methods.* 9:676–682. https://doi.org/10.1038/nmeth.2019

Schlager, M.A., H.T. Hoang, L. Urnavicius, S.L. Bullock, and A.P. Carter. 2014. In vitro reconstitution of a highly processive recombinant human dynein complex. *EMBO J.* 33:1855–1868. https://doi.org/10.15252/embj.201488792

Schliwa, M., and G. Woehlke. 2003. Molecular motors. *Nature.* 422:759–765. https://doi.org/10.1038/nature01601

Schroeder, C.M., and R.D. Vale. 2016. Assembly and activation of dynein-dynactin by the cargo adaptor protein Hook3. *J. Cell Biol.* 214:309–318. https://doi.org/10.1083/jcb.201604002

Shintani, M., M. Tada, T. Kobayashi, H. Kajiho, K. Kontani, and T. Katada. 2007. Characterization of Rab45/RASEF containing EF-hand domain and a coiled-coil motif as a self-associating GTPase. *Biochem. Biophys. Res. Commun.* 357:661–667. https://doi.org/10.1016/j.bbrc.2007.03.206

Simunovic, M., J.-B. Manneville, H.-F. Renard, E. Evergren, K. Raghunathan, D. Bhatia, A.K. Kenworthy, G.A. Voth, J. Prost, H.T. McMahon, et al. 2017. Friction Mediates Scission of Tubular Membranes Scaffolded by BAR Proteins. *Cell.* 170:172–184.e11. https://doi.org/10.1016/j.cell.2017.05.047

Srikanth, S., H.-J. Jung, K.-D. Kim, P. Souda, J. Whitelegge, and Y. Gwack. 2010. A novel EF-hand protein, CRACR2A, is a cytosolic Ca2+ sensor that stabilizes CRAC channels in T cells. *Nat. Cell Biol.* 12:436–446. https://doi.org/10.1038/ncb2045

Srikanth, S., K.-D. Kim, Y. Gao, J.S. Woo, S. Ghosh, G. Calmettes, A. Paz, J. Abramson, M. Jiang, and Y. Gwack. 2016. A large Rab GTPase encoded by CRACR2A is a component of subsynaptic vesicles that transmit T cell activation signals. *Sci. Signal.* 9:ra31. https://doi.org/10.1126/scisignal.aac9171

Srikanth, S., J.S. Woo, and Y. Gwack. 2017. A large Rab GTPase family in a small GTPase world. *Small GTPases.* 8:43–48. https://doi.org/10.1080/21541248.2016.1192921

Stinchcombe, J.C., and G.M. Griffiths. 2014. Communication, the centrosome and the immunological synapse. *Philos. Trans. R. Soc. Lond. B Biol. Sci.* 369:20130463. https://doi.org/10.1098/rstb.2013.0463

Urnavicius, L., K. Zhang, A.G. Diamant, C. Motz, M.A. Schlager, M. Yu, N.A. Patel, C.V. Robinson, and A.P. Carter. 2015. The structure of the dynactin complex and its interaction with dynein. *Science.* 347:1441–1446. https://doi.org/10.1126/science.aaa4080

Urnavicius, L., C.K. Lau, M.M. Elshenawy, E. Morales-Rios, C. Motz, A. Yildiz, and A.P. Carter. 2018. Cryo-EM shows how dynactin recruits two dyneins for faster movement. *Nature.* 554:202–206. https://doi.org/10.1038/nature25462

Vale, R.D. 2003. The molecular motor toolbox for intracellular transport. *Cell.* 112:467–480. https://doi.org/10.1016/S0092-8674(03)00111-9

Wilson, L.A., L. McKeown, S. Tumova, J. Li, and D.J. Beech. 2015. Expression of a long variant of CRACR2A that belongs to the Rab GTPase protein family in endothelial cells. *Biochem. Biophys. Res. Commun.* 456:398–402. https://doi.org/10.1016/j.bbrc.2014.11.095

Yap, K.L., J.B. Ames, M.B. Swindells, and M. Ikura. 1999. Diversity of conformational states and changes within the EF-hand protein superfamily. *Proteins.* 37:499–507. https://doi.org/10.1002/(SICI)1097-0134(19991115)37:3<499::AID-PROT17>3.0.CO;2-Y

Yi, J., X.S. Wu, T. Crites, and J.A. Hammer III. 2012. Actin retrograde flow and actomyosin II arc contraction drive receptor cluster dynamics at the immunolo. *Mol. Biol. Cell.* 23:834–852. https://doi.org/10.1091/mbc.e11-08-0731

Zhang, J., R. Qiu, H.N. Arst Jr., M.A. Peñalva, and X. Xiang. 2014. HookA is a novel dynein-early endosome linker critical for cargo movement in vivo. *J. Cell Biol.* 204:1009–1026. https://doi.org/10.1083/jcb.201308009

Zhang, K., H.E. Foster, A. Rondelet, S.E. Lacey, N. Bahi-Buisson, A.W. Bird, and A.P. Carter. 2017. Cryo-EM Reveals How Human Cytoplasmic Dynein Is Auto-inhibited and Activated. *Cell.* 169:1303–1314.e18. https://doi.org/10.1016/j.cell.2017.05.025